International Journal of Computer Applications (0975 - 8887)
Volume 187 - No.108, May 2026

Multi-Band RLS Estimation with Rank Two Updates: Application to Short-Term Temperature Forecast

Alexander Stotsky
Independent Researcher
Gothenburg, Sweden

ABSTRACT

Time series approximation is a key tool for predicting the future dynamics of complex systems, including climate behavior, financial markets and industrial processes. In practice, many multi-frequency signals display pronounced frequency separation among their components, a characteristic that severely limits the performance of standard approximation approaches. To address the limitations of conventional approaches, this paper introduces a novel multi-band recursive least squares method aimed at improving approximation and predictive accuracy. The proposed framework decomposes the signal spectrum into multiple frequency bands and performs independent parameter estimation within each band using customized window sizes and forgetting factors, thereby enabling significantly enhanced trade-off management across frequency scales. The proposed framework surpasses full-band estimation, where the signal bandwidth is handled as a unified frequency range, by delivering improved approximation and predictive accuracy. In addition, it reduces matrix dimensions and condition numbers, thereby increasing numerical robustness and reducing parameter variance. The recursive structure relies on rank two updates, ensuring convergence of both the inverses of the information matrices and the parameter estimation errors for each band. The key contribution of this paper lies in a Lyapunov based convergence analysis formulated for simplified error dynamics that characterize the dominant transient error mode. This mode is obtained through decomposition of the rank two increment matrix and its representation in dyadic form, which provides a structured basis for convergence assessment. The effectiveness of the proposed method is demonstrated through temperature prediction using high resolution observational data. The results confirm that multi-band predictions, optimized independently across frequency bands, offer improved accuracy compared with the conventional full-band model.

Keywords

multi-band recursive least squares estimation with rank two updates, simplified error models, Lyapunov analysis, Richardson correction algorithm & convergence rate improvement, short-term temperature forecast for control

1. PROCESSING OF TIME SERIES DATA

Approximation & Prediction. Approximation of time series data is commonly used to forecast the future behavior of various systems, such as weather patterns, financial markets, industrial processes and more. Many real-world multi-frequency signals are characterized by large disparities between constituent frequencies, which significantly degrades the performance of conventional approximation methods, [1], [2]. RLS (Recursive Least Squares) estimation with a moving window and exponential or segmented forgetting, [3],[4] allows flexibility in selecting window size and forgetting factor but remains inadequate for high performance multi-band estimation, which is crucial for accurate forecasting. In other words, full-band estimation without separation can combine signal modes, complicating the identification of individual factors. This requires the development of multi-band RLS estimation algorithms that partition the frequency range into smaller bands, improving model accuracy by adapting to specific frequency regions.

This paper introduces a novel multi-band least squares estimation approach in which the frequency range is divided by selecting suitable moving-window lengths. Larger windows correspond to low frequencies, while shorter windows capture high frequency components. The estimation performance is further optimized by selecting suitable forgetting factors. Each frequency band is estimated using the least squares algorithm, with its own window size and forgetting factor, significantly enhancing the ability to optimize the trade-offs for each band. They offer several computational advantages over full-band estimation, including smaller matrix dimensions, enhanced numerical stability due to lower condition numbers, reduced parameter variance, the ability to leverage parallel processing and more.

The algorithms are implemented recursively via rank two updates, ensuring convergence of both the information matrix inverses and the parameter estimation errors for each band. In this paper, Lyapunov convergence analysis is conducted on simplified error models that capture the dominant mode of the error transients. This primary mode is identified through decomposition of the rank two increment matrix and its representation in dyadic form, which facilitates the convergence analysis. In other words, for the purpose of simplifying the analysis, the rank two updates are approximated as rank one updates. The effectiveness of this approach is confirmed by simulations.

The nested structure of multi-band estimation can lead to the propagation of oscillatory behavior in estimation errors, where fluctuations in the low-frequency band may influence higher-frequency bands. This paper demonstrates that the transient performance can be enhanced using the Richardson correction algorithm, while the computational efficiency of the approach can be improved by leveraging the convergence properties of the gain matrix.

Temperature Forecast. The proposed approach is evaluated on a temperature forecasting problem using high resolution temperature

readings recorded every ten minutes,[5]. The temperature time series exhibits seasonal, weekly, and daily periodicities, with each cycle corresponding to a distinct component of the signal. The signal was decomposed into two frequency bands: the lower-frequency band captures the weekly and daily periodicities, while the higher-frequency band encompasses components influenced by factors such as weather patterns, human activities, and environmental conditions. It has been demonstrated that recursive multi-band temperature estimation with rank two updates significantly improves both approximation and forecasting performance when compared to full-band estimation.

Notice that the computational efficiency achieved through the recursive structure of these algorithms with rank two updates is essential for temperature forecasting. Weather prediction services must deliver updates to millions of phones, computers and electronic control units simultaneously. For example, in energy and building automation systems, predicted temperature is used as an exogenous input in anticipatory control algorithms. Short term forecasts of outdoor and indoor temperature allow the controller to anticipate future thermal loads and optimize heating, cooling, and airflow over a prediction horizon. This enables proactive actions, such as pre-cooling or load shifting, to maintain comfort while reducing energy consumption. At the grid level, temperature predictions support demand forecasting and generation scheduling, helping energy providers balance supply and demand under operational constraints. Outdoor activities, agriculture, transportation, and construction can also use this near-term forecast to prevent damage, improve safety, or adjust operations efficiently.

Even minor fluctuations in temperature can be critical during extreme weather events such as heatwaves or frost, as early detection enables timely precautionary measures. Moreover, short term temperature forecasts contribute to larger-scale predictive models, enhancing the accuracy of long term weather predictions. Delays in prediction generation can hinder proactive control strategies, increase the risk of service failures, overload systems, and ultimately raise operational costs while degrading overall performance. In contrast, fast recursive prediction methods with rank two updates enable simultaneous service to a larger number of users, improve system reliability, and significantly reduce cloud computing expenses. This paper therefore focuses on one-hour-ahead temperature predictions, which are essential for rapid decision making, energy efficiency, safety, and effective operational planning.

2. NESTED RLS ALGORITHMS WITH RANK TWO UPDATES

Suppose that the oscillating signal y_k can be presented as a sum of $m > 1$ frequency-band components $p_{i,k}$ contaminated with white Gaussian zero mean noise ξ_k :

$$y_k = \sum_{i=1}^{m} p_{i,k} = \sum_{i=1}^{m} \varphi_{i,k}^T \theta_{i*} + \xi_k,\ p_i = \varphi_{i,k}^T \theta_{i*} \tag{1}$$

$$\varphi_{i,k}^T = [cos(q_{i,1}k)\ sin(q_{i,1}k)\ \ldots\ cos(q_{i,h_i}k)\ sin(q_{i,h_i}k)] \tag{2}$$

where each band $i = 1, \ldots, m$ is represented by its own harmonic regressor vector $\varphi_{i,k}$ that contains h_i distinct frequencies and unknown parameter vector θ_{i*}, $k = 1, 2, ...$ The first band encompasses the lower frequencies, capturing the low frequency components, while the m-th band corresponds to the upper end of the spectrum, representing the highest frequencies. The number of frequencies is not necessarily uniform across bands.

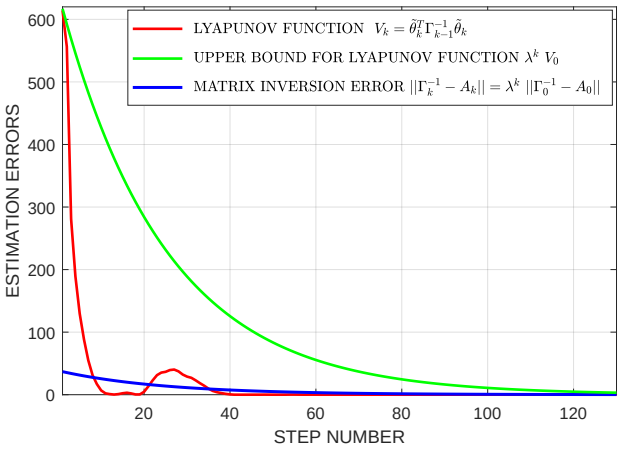

Fig. 1. The figure compares the Lyapunov function (red line), its upper bound (green line), and the matrix inversion error (blue line), revealing that the Lyapunov based bound is loose.

Given the significant frequency differences across bands, each band is independently estimated within a window of size w_i tailored to its specific frequency range. A band-specific forgetting factor $0 < \lambda_i < 1$ is also used to downweight past data, allowing for more accurate band-wise estimates that reflect the structure of the signal. The estimation relies on the recursive least squares algorithm with rank two updates, as outlined below:

$$\hat{y}_{1,k} = y_k,\ i = 1 \tag{3}$$

$$\Gamma_{i,k} = \frac{1}{\lambda_i} [\Gamma_{i,k-1} - \Gamma_{i,k-1} Q_{i,k} S_{i,k}^{-1}\ Q_{i,k}^T \Gamma_{i,k-1}] \tag{4}$$

$$\theta_{i,k} = \theta_{i,k-1} - \Gamma_{i,k-1} Q_{i,k}\ S_{i,k}^{-1}\ [Q_{i,k}^T \theta_{i,k-1} - \tilde{y}_{i,k}] \tag{5}$$

$$Q_{i,k} = [\varphi_{i,k}\ \sqrt{\lambda_i^{w_i}} \varphi_{i,k-w_i}] \tag{6}$$

$$\tilde{y}_{i,k}^T = [\hat{y}_{i,k}\ \sqrt{\lambda_i^{w_i}} \hat{y}_{i,k-w_i}] \tag{7}$$

$$S_{i,k} = \lambda_i D + Q_{i,k}^T\ \Gamma_{i,k-1}\ Q_{i,k} \tag{8}$$

$$\hat{y}_{i+1,k} = \hat{y}_{i,k} - \hat{p}_{i,k},\ \hat{p}_{i,k} = \varphi_{i,k}^T \theta_{i,k},\ \ i = i + 1 \tag{9}$$

where $\Gamma_{i,k}$ and $\theta_{i,k}$ are estimates of the inverse of the information matrix and parameter vector respectively for each band. Each algorithm is characterized by the regressor matrix (stack of column regressor vectors) $Q_{i,k}$, update matrix $S_{i,k}$, signature matrix $D = \text{diag}[1, -1]$ and the augmented output for each band $\tilde{y}_{i,k}$, [3]. The multicomponent least squares algorithm proceeds as follows. In the first stage, the estimation of the low frequency band is performed, wherein the measured signal y_k is directly utilized by the estimator (4) - (8), $i = 1$. The estimation procedure employs a sufficiently large window size, w_1 together with a forgetting factor, λ_1 whose value is chosen to be close to unity. Such a selection of estimation parameters facilitates the effective extraction of the low frequency components of the signal, $\hat{p}_{1,k} = \varphi_{1,k}^T \theta_{1,k}$.

In the subsequent stage, a virtual output is computed by subtracting the estimated low frequency band from the original signal, y_k using (9), $\hat{y}_{2,k} = y_k - \hat{p}_{1,k}$. This operation isolates the residual signal containing higher-frequency components, which are then estimated by the algorithm (4) - (8) with an incremented index $i = 2$. To

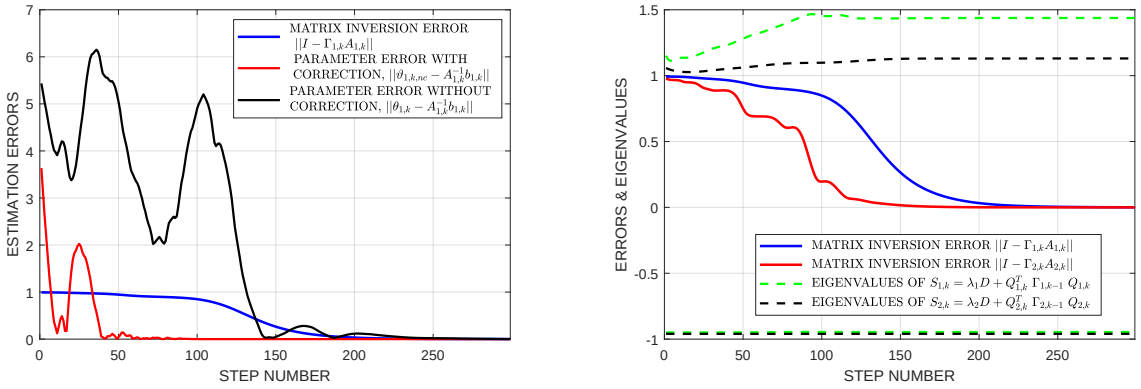

Fig. 2. The Figure 2(a) illustrates the convergence of the parameter errors for low frequency band without correction $||\theta_{1,k} - A_{1,k}^{-1}b_{1,k}||$ (black line), where $\theta_{1,k}$ is updated according to (5) and the parameter error with correction $||\vartheta_{1,k,nc} - A_{1,k}^{-1}b_{1,k}||$ (red line), where $\vartheta_{1,k,nc}$ is updated according to (23) for five correction steps, $n_c = 5$.
The matrix inversion errors for the low- and high-frequency bands are shown in Figures 2(a) and 2(b), plotted in blue and red, respectively. Figure 2(b) also presents the eigenvalues of the update matrices defined in (8) for both bands.

enhance the accuracy and responsiveness of the estimation at this stage, a shorter window $w_2 \ll w_1$ and typically a smaller forgetting factor $\lambda_2 \leq \lambda_1$ are used. This procedure is repeated for m bands, thereby constructing the model (10) for the multi-band signal (1) as follows:

$$\hat{y}_k = \hat{p}_{1,k} + \hat{p}_{2,k} + \ldots + \hat{p}_{m,k} = \sum_{i=1}^{m} \hat{p}_{i,k} \tag{10}$$

3. LYAPUNOV CONVERGENCE ANALYSIS USING SIMPLIFIED ERROR MODELS

The error model associated with (4) - (8) (where the band index i is omitted for simplicity in this section) can be written in the following form :

$$\Gamma_k = \frac{1}{\lambda}\left[\Gamma_{k-1} - \Gamma_{k-1}Q_k S_k^{-1}\, Q_k^T \Gamma_{k-1}\right] \tag{11}$$

$$\tilde{\theta}_k = (I - \Gamma_{k-1}Q_k\, S_k^{-1}Q_k^T)\,\tilde{\theta}_{k-1},\ \tilde{\theta}_k = \theta_k - \theta_* \tag{12}$$

$$Q_k \underbrace{\left[\lambda D + Q_k^T\,\Gamma_{k-1}\,Q_k\right]^{-1}}_{=S_k^{-1}} Q_k^T \approx \alpha_k\, v_k v_k^T \tag{13}$$

$$\Gamma_k = \frac{1}{\lambda}\left[\Gamma_{k-1} - \Gamma_{k-1}\alpha_k v_{i,k} v_{i,k}^T \Gamma_{k-1}\right] \tag{14}$$

$$\Gamma_k^{-1} = \lambda\left[\Gamma_{k-1}^{-1} + \frac{\alpha_k\, v_k v_k^T}{1 - \alpha_k v_k^T \Gamma_{k-1} v_k}\right],\quad \Gamma_k\Gamma_k^{-1} = I \tag{15}$$

$$\tilde{\theta}_k = (I - \alpha_k \Gamma_{k-1} v_k v_k^T)\,\tilde{\theta}_{k-1} \tag{16}$$

where $\tilde{\theta}_k$ is the parameter mismatch. The derivation of error model (11),(12) can be found in [3]. In this study, the rank two increment matrix $Q_k\, S_k^{-1} Q_k^T$ is expressed in dyadic form in (13) through the outer product of the orthonormal eigenvector v_k, ($||v_k|| = 1$) linked to the largest eigenvalue $\alpha_k > 0$, yielding a physically intuitive decomposition (see Appendix for a numerical example and [6]).
The rank one update applied to the gain matrix in (14) is an approximation of the rank two update given in (11). Using the matrix inversion lemma, equation (15) is obtained by inverting the gain matrix given in equation (14), yielding $\Gamma_k\Gamma_k^{-1} = I$, where I denotes the identity matrix.
Finally, the error model (16) is the rank one approximation of the rank two model (12), which captures the dominant component of the transient, keeping the trajectories of both models close.
The parameter convergence can be established using the Lyapunov function $V_k = \tilde{\theta}_k^T \Gamma_k^{-1} \tilde{\theta}_k$, where Γ_k^{-1} satisfies (15). Evaluation of this function along the solution of (16) yields:

$$V_k = \lambda V_{k-1} - \lambda\,\alpha_k\,(\tilde{\theta}_{k-1}^T v_k)^2 \tag{17}$$

$$V_k \leq \lambda V_{k-1},\quad V_k \leq \lambda^k V_0,\quad 0 < \lambda < 1 \tag{18}$$

Equation (17) shows that each update produces a strictly positive decrease in the Lyapunov function, proportional to the squared parameter error projected along eigenvector v_k. The last step is to demonstrate that the convergence of the Lyapunov function necessarily results in convergence of the parameter error.
The convergence of the gain matrix Γ_k to the inverse of information matrix A_k defined in (20) can be established using the following simplified model:

$$\Gamma_k^{-1} \approx \lambda\,\Gamma_{k-1}^{-1} + Q_k\, D\, Q_k^T \tag{19}$$

$$A_k = \lambda\, A_{k-1} + Q_k\, D\, Q_k^T \tag{20}$$

$$\Gamma_k^{-1} - A_k \approx \lambda\,[\Gamma_{k-1}^{-1} - A_{k-1}] \tag{21}$$

$$\Gamma_k^{-1} - A_k \approx \lambda^k\,[\Gamma_0^{-1} - A_0],\quad \Gamma_0^{-1}, A_0 > 0 \tag{22}$$

Applying the Neumann series expansion to (13) indicates that $S_k^{-1} \approx \lambda^{-1} D$ under the condition $\|Q_k^T\,\Gamma_{k-1}\,Q_k\| \ll \lambda$. Under this approximation, equation (19) is obtained from (15) provided that $\alpha_k\, v_k^T \Gamma_{k-1}^{-1} v_k \ll 1$. The matrix inversion error model (21) is obtained by subtracting (20), which is derived in [3], [9], from (19). The error model (22) implies that $\Gamma_k^{-1} \to A_k$ as $k \to \infty$. Subsequently, $\Gamma_k \to A_k^{-1}$ since the information matrix is positive definite for systems with harmonic regressor, [7]. Thus the convergence of the parameter error follows from the convergence of the Lyapunov

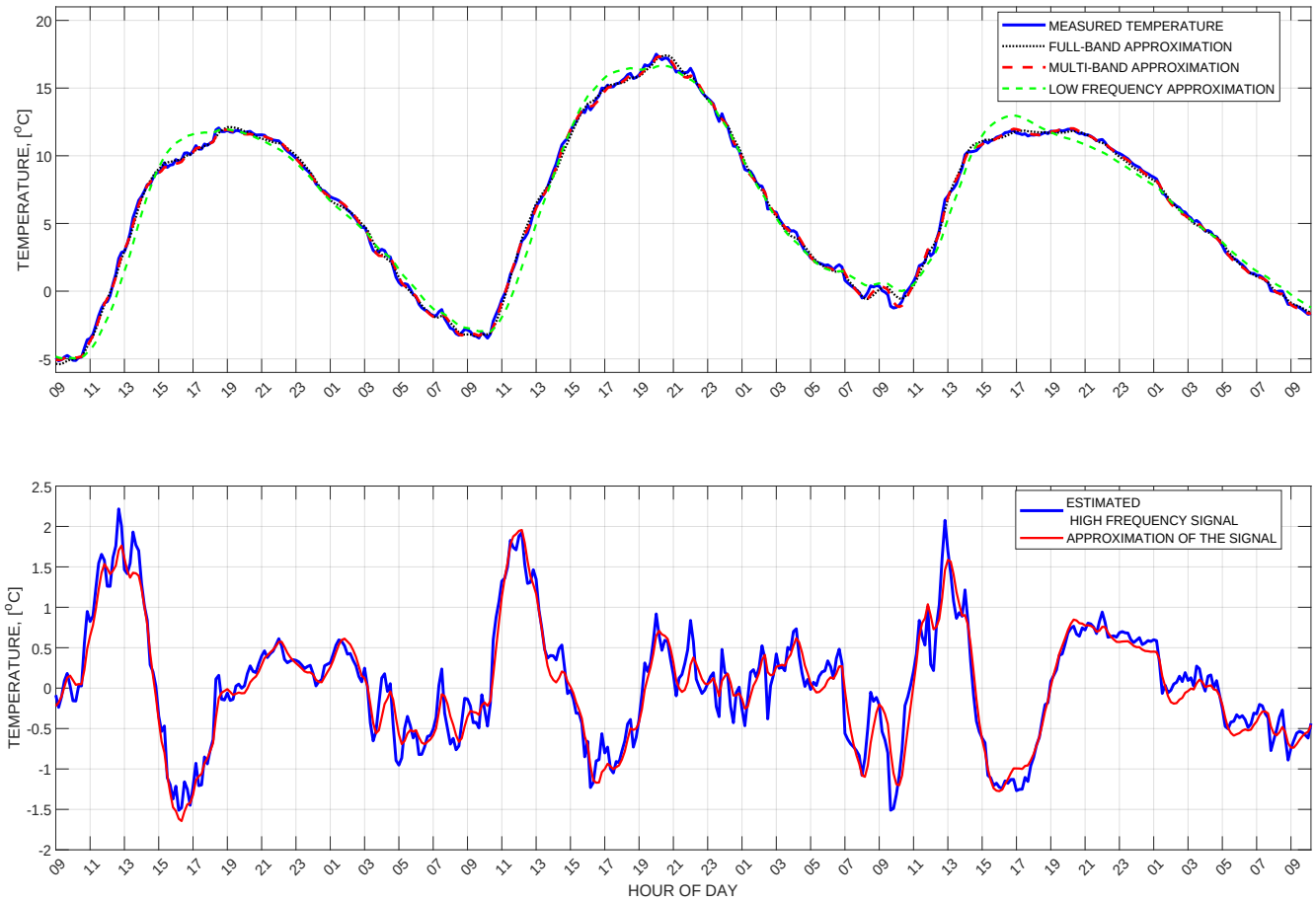

Fig. 3. This figure illustrates the multi-band estimation concept. The measured temperature signal (blue line, first plot) is first approximated using low frequency components, $h_1 = 2$ (green line), estimated by the RLS algorithm with rank two updates, window size $w_1 = 250$, and forgetting factor $\lambda_1 = 0.96$. The high frequency component ($h_2 = 4$) defined as the difference between the measured signal and its low-frequency approximation, is shown in the second plot (blue line) and is approximated using the RLS algorithm with rank two updates, window size $w_2 = 130$, and forgetting factor $\lambda_2 = 0.95$ (red line). The resulting multi-band approximation, obtained by summing the low- and high-frequency components, is shown by the red line in the first plot and is compared with the full-band approximation with six frequencies, estimated using the RLS algorithm with rank two updates, window size $w = 144$, and forgetting factor $\lambda = 0.99$ (black line). As demonstrated by the histograms in Figure 4, the multi-band frequency estimation achieves superior approximation performance compared to the full-band approach.

function.

The proposed convergence analysis holds for all bands and extends naturally to the RLS algorithms with low rank updates proposed in [4]. Nevertheless, it is important to recognize that convergence results derived from simplified models may not be exact.

Figure 1 illustrates the evolution of the Lyapunov function V_k (red line) and its associated upper bound (green line), together with the matrix inversion error (blue line). The results clearly show that the Lyapunov based bound $\lambda^k V_0$ substantially overestimates the actual error, indicating a loose and highly conservative approximation.

4. CONVERGENCE RATE & EFFICIENCY IMPROVEMENT

The least squares solution minimizes the cost function associated with the error between measured and estimated outputs for each band. The minimization is associated with the normal equation $A_{i,k}\theta_{i,k} = b_{i,k}$ where $A_{i,k}$ and $b_{i,k}$ are information matrix and observation vector respectively for each band, [3]. Recursive procedures (4) and (5) provide estimates for the inverse of the information matrix and the parameter vector, respectively, ensuring that the normal equation holds. The hierarchical nature of multi-band estimation can cause oscillatory estimation errors to propagate between frequency bands, with low frequency fluctuations impacting higher-frequency components. This paper shows that transient performance

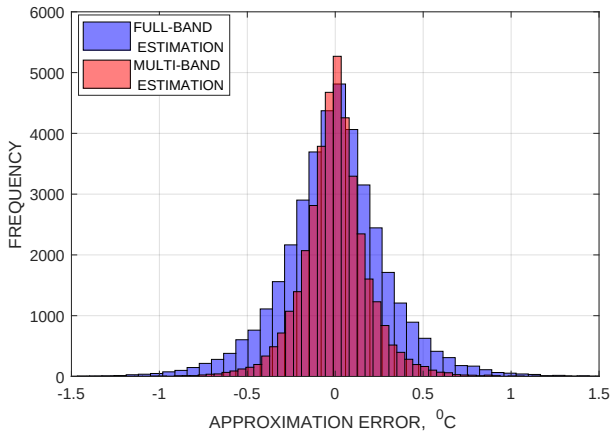

Fig. 4. The blue histogram represents the approximation error of the full-band estimation, while the red histogram corresponds to the multi-band approximation. The multi-band approach significantly improves approximation performance.

can be improved by applying the Richardson correction algorithm, [8], [9], which minimizes the mismatch associated with the normal equation as follows:

$$\vartheta_j = \vartheta_{j-1} - (I + F_{i,k})\,\Gamma_{i,k}\,(A_{i,k}\,\vartheta_{j-1} - b_{i,k}) \qquad (23)$$
$$F_{i,k} = I - \Gamma_{i,k}A_{i,k},\ \Gamma_{i,0} = 2I/||A_{i,0}||_\infty$$
$$\rho(I - \Gamma_{i,0}A_{i,0}) < 1,\ \vartheta_0 = \theta_{i,k}$$

where $F_{i,k}$ is the inversion error, $\rho(\cdot)$ is the spectral radius, $j = 1, ..., n_c$, n_c is the number of the correction steps. Such corrections are necessary for accuracy improvement in cases involving ill-conditioned information matrices.
Figure 2(a) demonstrates the convergence behavior of the matrix inversion error and the ability of the Richardson algorithm, over five correction steps, to reduce oscillations in the estimation errors.
Interestingly enough that the same correction algorithm can be used instead of (5) as follows:

$$\theta_{i,k} = \theta_{i,k-1} - \Gamma_{i,k}\,(A_{i,k}\,\theta_{i,k-1} - b_{i,k}) \qquad (24)$$

By incorporating the error $\theta_{i,k-1} - A_{i,k}^{-1}b_{i,k}$ the algorithm reduces computational complexity, which is essential for on-board applications, and improves estimation accuracy, leveraging the convergence of the matrix inversion error $F_{i,k} \to 0$.
Moreover, after a brief initial transient, the eigenvalues and elements of the update matrices for each band settle to fixed values, as shown in Figure 2(b). Pre-computed inverses can then be employed in recursive estimation algorithms (4) and (5), reducing computational burden.

5. SHORT-TERM TEMPERATURE FORECASTS

Temperature time series (as acquired in [5]) display seasonal, weekly, and daily periodicities, which can be decomposed into separate components of the signal. Components of temperature time series at frequencies higher than the daily cycle are primarily influenced by sub-daily fluctuations, including rapid meteorological events (cloud cover changes, wind shifts, frontal passages, etc), short-term radiative effects, and localized anthropogenic factors. These high frequency variations correspond to higher-frequency components in the spectrum, which can introduce significant signal complexity. Analyzing these components requires application of multi-band techniques. In other words, the temperature signal naturally splits into two frequency bands: the low frequency band, which captures weekly and daily periodicities, and the high frequency band, which encompasses faster sub-daily fluctuations.
In multi-band estimation, the estimator adjusts to the unique characteristics of each band, enhancing the overall model fit and accuracy by more effectively capturing the distinct patterns. In contrast, full-band estimation can "mix" these patterns, making it more challenging to distinguish and identify the individual contributing factors. Multi-band estimation provides improved accuracy by customizing the estimator for each band through an optimal selection of window size and forgetting factor.
Figure 3 illustrates the multi-band estimation approach. The measured temperature (blue line, first plot) is initially approximated using low frequency components (green line), which capture weekly and daily periodicities. The high frequency band, representing sub-daily fluctuations, is obtained by subtracting the low-frequency approximation from the measured signal. This high frequency component is shown in the second plot (blue line) and is further approximated using four distinct high frequency components (red line). The resulting multi-band approximation, obtained by summing the low- and high-frequency components (red line, first plot), is compared with the six-frequency full-band approximation (black line). As shown in Figure 4, the multi-band approach outperforms the full-band method by enabling RLS estimation in each band with window sizes and forgetting factors tailored to the frequency content of the signal.
One-hour-ahead Predictions. After validating the temperature time series model, it can be utilized to forecast future values by propagating the model forward in time, enabling the prediction of future temperature trends. The reliability and precision of predictions are contingent upon the choice of model, as different modeling approaches demonstrate distinct levels of forecasting accuracy. Figure 5(a) presents one-hour-ahead predictions for different models, facilitating a comparison of forecasting accuracy for: (a) the low frequency model, which captures only weekly and daily periodicities, (b) the model validated using the full-band method, and (c) the multi-band model. The figure illustrates the low prediction accuracy of the low frequency model, as evident from the comparison between the cyan line (predicted temperature) and the blue line (actual temperature at the forecast time). Prediction accuracy may be enhanced by accounting for the high frequency components of the signal, which can be achieved through various approaches. Nevertheless, predictions based on the full-band model (black line) do not exhibit a substantial improvement in accuracy. The multi-band approach decomposes the signal into low- and high-frequency components, allowing predictions to be performed separately for each band. By selecting window sizes and forgetting factors independently for different components, the prediction model can be better calibrated for each frequency range. This is illustrated by the comparison between the multi-band model predictions (red line) and the actual measurements (blue line). The corresponding histograms of prediction errors for the multi-band and full-band models are presented in Figure 5(b), demonstrating a clear improvement in prediction accuracy.
Confidence Interval Approach for Prediction. Temperature readings taken at ten-minute intervals exhibit high frequency noise that periodic functions are unable to model. This noise arises from microscale atmospheric and environmental processes, including turbulent mixing in the near-surface air, rapid fluctuations in wind speed and direction, and changes in daytime solar radiation and cloud cover. Additional short-term variability is introduced by longwave

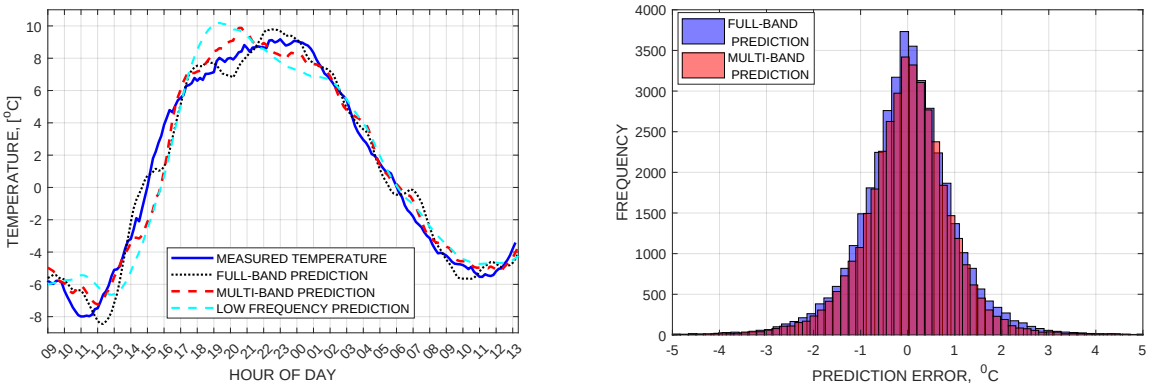

(a) (b)

Fig. 5. Figure 5(a) illustrates the comparison between temperature predictions from the low-frequency (cyan), full-band (black), and multi-band (red) models and the observed temperature (blue) at the target time. Prediction error histograms for the multi-band and full-band models are presented in Figure 5(b).

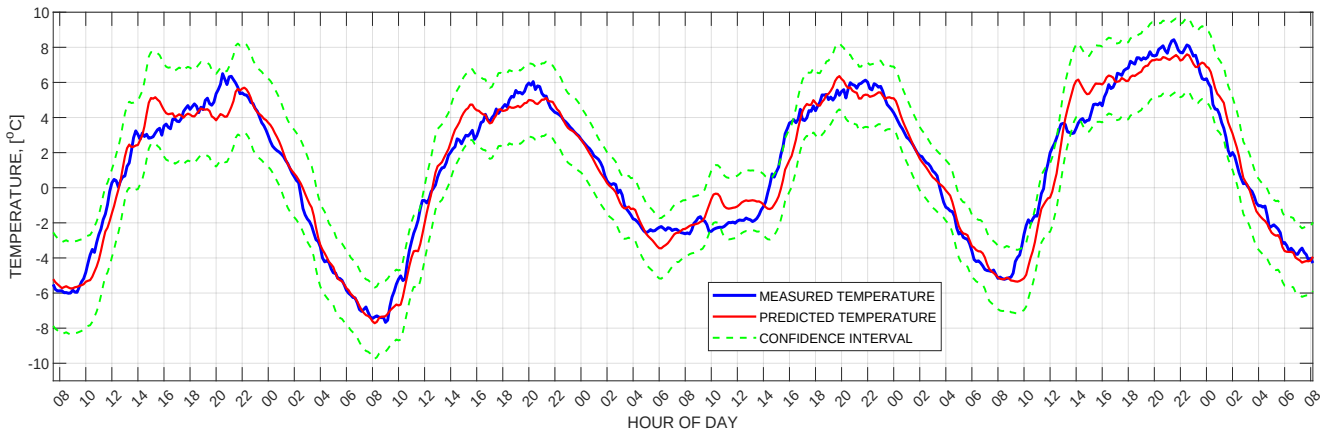

Fig. 6. The figure illustrates the effectiveness of the confidence interval method, showing measured temperature (blue), one-hour-ahead predictions (red), and three-sigma confidence prediction interval (green). The alignment of almost all measured temperatures with the predicted confidence interval demonstrates the high fidelity of the prediction and noise models.

radiation emitted from surrounding surfaces, while local disturbances, such as nearby buildings, roads, and human activities, can produce brief thermal spikes. Moreover, the ten-minute temporal resolution causes aliasing of high frequency components, which contaminates the series with noise.

Prediction models cannot directly resolve high frequency temperature fluctuations, but such variations are captured indirectly through the uncertainty of the predicted mean temperature, represented by confidence intervals estimated from historical data. If this variability remains relatively stable over time, these intervals can also inform confidence bounds for future predictions, [4], [10]. Figure 6 illustrates the effectiveness of the confidence interval method, showing measured temperature (blue line), one-hour-ahead predictions (red line), and the three-sigma confidence prediction interval (green lines). Nearly all measured temperature values lie within the confidence interval of the predicted temperatures, indicating the high accuracy of both the prediction and noise models.

6. CONCLUSIONS & OUTLOOK

This paper introduced new multi-band recursive least squares framework with rank two updates, where the signal spectrum is divided into multiple frequency bands, and window sizes and forgetting factors are tailored for each band, enabling efficient and accurate parameter estimation. By partitioning the signal into multiple frequency bands and optimizing predictions for each, the algorithms outperform traditional full-band prediction. By reducing matrix dimensions and condition numbers, this strategy improves numerical stability, enhances approximation and prediction accuracy, and ultimately reduces parameter variance.

This paper applies the novel method to convergence analysis utiliz-

ing simplified error models that capture only the dominant mode of error transients. The analysis verifies convergence of both the inverse information matrices and the parameter errors for every band. Since convergence analysis with simplified models may not be fully accurate, refining approximation methods represents a critical challenge for further development.
The methodology's practical effectiveness was confirmed through high resolution temperature prediction, where frequency-specific multi-band models consistently surpass the predictive accuracy of full-band approaches.
Further improvements can be achieved by enhancing the approximation performance of the recursive least squares algorithms for each band through segmentation of the forgetting profiles, [4].

Declarations

This research was not supported by any organization.

7. REFERENCES

[1] Xiong Y. & Wen Y. (2025). *Non-stationary time series forecasting based on Fourier analysis and cross attention mechanism*. arXiv:2505.06917v1 [cs.LG]
https://arxiv.org/pdf/2505.06917

[2] Stotsky A. (2022). *Simultaneous frequency and amplitude estimation for grid quality monitoring : new partitioning with memory based Newton-Schulz corrections*. IFAC PapersOnLine, 55(9), 42-47.
https://doi.org/10.1016/j.ifacol.2022.07.008

[3] Stotsky A. (2025). *Recursive least squares estimation with rank two updates*. Automatika, 66(4),619-624.
https://doi.org/10.1080/00051144.2025.2517431

[4] Stotsky A. (2025) *Accelerating with low rank updates: RLS estimation with segmentation of the forgetting profile*. International Journal of Computer Applications (0975 - 8887), 187(54), 1–5.
https://doi.org/10.5120/ijca2025925940

[5] Kolle O. (2025). *Documentation of the weather station on top of the roof of the institute building of the Max-Planck-Institute for biogeochemistry. Max-Planck-Institute for biogeochemistry*. Techinical report.
https://www.bgc-jena.mpg.de/wetter/Weatherstation.pdf

[6] Eckart C. & Young G. (1936). *The approximation of one matrix by another of lower rank*. Psychometrika 1, 211–218.
https://doi.org/10.1007/BF02288367

[7] Stotsky A. (2010). *Recursive trigonometric interpolation algorithms*. Journal of Systems and Control Engineering, 224(1),65-77.
https://doi.org/10.1243/09596518JSCE823

[8] Stotsky A. (2022). *Recursive versus nonrecursive Richardson algorithms: systematic overview, unified frameworks and application to electric grid power quality monitoring*. Automatika,63(2),328-337.
https://doi.org/10.1080/00051144.2022.2039989

[9] Stotsky A. (2022). *Recursive estimation in the moving window: efficient detection of the distortions in the grids with desired accuracy*. Journal of Advances in Applied and Computational Mathematics,9, 181-191.
https://doi.org/10.15377/2409-5761.2022.09.14

[10] Stotsky A. (2025). *Detection and control of credit card fraud attacks in sliding window with exponential forgetting*. International Journal of Computer Applications (0975 - 8887), 186(74),9–15.
https://doi.org/10.5120/ijca2025924619

Appendix: Optimal Rank One Approximation of Rank Two Matrices - Numerical Example

A real symmetric rank two matrix admits an optimal rank one approximation (with respect to the Frobenius norm) by projecting onto the eigenvector associated with its largest-magnitude eigenvalue. The resulting approximation error is the square of the non-dominant eigenvalue. Consider the rank two increment matrix defined in (13):

$$Q_k\, S_k^{-1} Q_k^T = \begin{bmatrix} 0.882359937168498 & -0.044026886203692 & 0.830176202206646 & -0.302169875412764 \\ -0.044026886203692 & 0.002158193728505 & -0.041411751395377 & 0.015114044186660 \\ 0.830176202206647 & -0.041411751395377 & 0.781075341576455 & -0.284310009802377 \\ -0.302169875412764 & 0.015114044186660 & -0.284310009802377 & 0.103445042801232 \end{bmatrix}$$

whose only nonzero eigenvalues are $\alpha_k = 1.769115436898466$ and $\beta_k = -7.6921623774 \times 10^{-5}$.
In the Frobenius norm sense, this matrix admits an optimal rank one approximation by preserving only the leading eigenvalue α_k and eigenvector v_k:

$$\alpha_k\, v_k v_k^T = \begin{bmatrix} 0.882359937168756 & -0.044026883050608 & 0.830176201280962 & -0.302169878414634 \\ -0.044026883050608 & 0.002196797870687 & -0.041423084826894 & 0.015077291406798 \\ 0.830176201280962 & -0.041423084826894 & 0.781078668853340 & -0.284299219895127 \\ -0.302169878414634 & 0.015077291406798 & -0.284299219895127 & 0.103480033005682 \end{bmatrix}$$

where $v_k = [-0.706227792440088\ 0.035238463483074\ -0.664460705058984\ 0.241852284068335]^T$, $\|v_k\| = 1$. An element-wise comparison of two matrices shows that $Q_k\, S_k^{-1} Q_k^T \approx \alpha_k\, v_k v_k^T$.